# **Nanoscale**



## COMMUNICATION

View Article Online



Cite this: Nanoscale, 2018, 10, 13924

Received 12th April 2018, Accepted 6th July 2018 DOI: 10.1039/c8nr02994f

rsc.li/nanoscale

# Tunable thermal conductivity of $\pi$ -conjugated two-dimensional polymers†

Hao Ma, Da Erica O'Donnel Da and Zhiting Tian \*\* \*a,b,c

Two-dimensional (2D) polymers are organic analogues of graphene. Compared to graphene, 2D polymers offer a higher degree of tunability in regards to structure, topology, and physical properties. The thermal transport properties of 2D polymers play a crucial role in their applications, yet remain largely unexplored. Using the equilibrium molecular dynamics method, we study the in-plane thermal conductivity of dubbed porous graphene that is comprised of  $\pi$ -conjugated phenyl rings. In contrast to the conventional notion that  $\pi$ -conjugation leads to high thermal conductivity, we demonstrate, for the first time, that  $\pi$ -conjugated 2D polymers can have either high or low thermal conductivity depending on their porosity and structural orientation. The underlying mechanisms that govern thermal conductivity were illustrated through phonon dispersion. The ability to achieve two orders of magnitude variance in thermal conductivity by altering porosity opens up exciting opportunities to tune the thermal transport properties of 2D polymers for a diverse array of applications.

#### 1. Introduction

Since the discovery of graphene, there has been interest in synthesizing an organic analogue as a two-dimensional (2D) polymer. 2D polymers are flat sheets composed of periodic networks or repeating organic units, arranged in two orthogonal directions. They have the great potential to possess novel physical properties that are inherited from  $\pi$ -conjugation, ordered molecular crystals, and 2D confinement. While the zero bandgap has limited the potential use of graphene as a semiconductor in electronic devices, 2D polymers possess a tunable bandgap. They are not limited to the pure sp² hybridization of graphene, which allows their electrical and optical

properties to be tuned through alteration of the molecular structure of their building units and the number of double and triple bonds.<sup>2</sup> For example, 2D polymers have displayed both semiconducting behavior and metallic conductivity.<sup>3</sup> Because of this flexibility, 2D polymers have a wide array of potential applications in molecular and organic electronics, sensors, catalysis, molecular recognition, optoelectronic devices, energy storage and conversion, and membrane separation.<sup>4-6</sup> The thermal transport properties of 2D polymers play an important role in these applications, yet, remain largely unexplored.<sup>7</sup>

Dubbed porous graphene (DPG), which contains regular 2D poly(*p*-phenylene) (PPP) networks with atomic scale pores, is a graphene-like 2D polymer that has attracted special attention. Experimentally, DPG has been successfully synthesized using metal substrates as templates. <sup>8,9</sup> Theoretical research has been conducted to understand the structural and electronic properties of DPG. <sup>10–14</sup> DPG is a semiconductor with a wide band gap, which can be potentially applied to nanoelectronics. <sup>12</sup> Also, DPG showed high selectivity for H<sub>2</sub> permeability because of its porous structure, providing a great opportunity for hydrogen purification and storage. <sup>13,14</sup>

In this work, we carried out the first thermal conductivity study of DPG using equilibrium molecular dynamics (EMD) simulations. We compared the thermal conductivity of DPG to graphene and DPG structures with different porosities, elucidated the effects of porosity and structure orientation on thermal conductivity, and supported our explanation by detailed calculations of phonon dispersion. We also showed the temperature dependence of thermal conductivity and revealed the crystallinity change with porosity. Two highlights of our research are that (1)  $\pi$ -conjugation does not necessarily lead to high thermal conductivity in 2D polymers and (2) the thermal conductivity of DPG is highly tunable over two orders of magnitude. Our results provide useful insights into the fundamental mechanisms that govern the thermal conductivity of 2D polymers, allowing the rational design of 2D polymers to achieve desired thermal transport properties.

<sup>&</sup>lt;sup>a</sup>Department of Mechanical Engineering, Virginia Tech, Blacksburg, Virginia 24061, USA. E-mail: zhiting@cornell.edu

<sup>&</sup>lt;sup>b</sup>Macromolecules Innovation Institute, Virginia Tech, Blacksburg, Virginia 24061, USA
<sup>c</sup>Sibley School of Mechanical and Aerospace Engineering, Cornell University, Ithaca,
NY 14853, USA

<sup>†</sup>Electronic supplementary information (ESI) available. See DOI: 10.1039/c8nr02994f

Nanoscale Communication

#### 2. Simulation method

All 2D polymers were built in the BIOVIA Materials Studio, 15 and the unit cells<sup>16</sup> of DPG are shown in Fig. 1. The area A in the x-y plane of the supercell for all structures in this study was kept at 92.4 Å  $\times$  92.4 Å, which is large enough to rule out size effects. The length of the supercell in the z direction was set to 40 Å to avoid interaction between neighboring layers. Periodic boundary conditions were applied in the x, y, and zdirections. We optimized all structures using Polymer Consistent Force-Field (PCFF) within the Materials Studio. PCFF, a class II potential that includes anharmonic bonding terms, 17,18 is intended for applications in polymers and organic materials. 19-21 EMD simulations<sup>22</sup> were performed with the PCFF potential using LAMMPS.<sup>23</sup> EMD simulations do not involve a temperature gradient, and thermal conductivity (k) is calculated by the autocorrelation of instantaneous heat flux through the Green-Kubo formula based on linear response theory.<sup>24,25</sup>

$$k(T) = \frac{1}{Vk_{\rm B}T^2} \int_0^\infty \langle \vec{J}(t) \cdot \vec{J}(t+\tau) \rangle \mathrm{d}\tau$$
 (1)

where k is the thermal conductivity, V is the volume of the simulated system,  $k_{\rm B}$  is the Boltzmann constant, T is the absolute temperature, J is the heat flux, and  $\tau$  is the delay time. Ten ensembles with different random initial velocities were simulated for each structure at a given temperature, from which the average k values were calculated. We chose 0.5 fs for the time step and 10 Å for the cutoff distance for the Lennard-Jones interaction. We first relaxed the system in a canonical ensemble (NVT) and a microcanonical ensemble (NVE), each for 500 ps. Heat flux data were then collected in an NVE ensemble for another 500 ps. The thicknesses of 2D polymers were calculated by the maximum difference of atomic coordinates along the z direction at the equilibrium state.

The spectral energy density (SED) method was used to calculate phonon dispersion.<sup>26-29</sup> Atomic velocities were collected using MD simulation for 100 ps. SED is defined by

$$\Phi(q,\omega) = \frac{1}{4\tau_0 \pi} \sum_{\alpha} \sum_{b}^{B} \frac{m_b}{N} \left| \int_0^{\tau} \sum_{l}^{N} \dot{u}_{\alpha} \binom{l}{b}, t \exp(i \mathbf{q} \cdot \mathbf{r}_l - i \omega t) dt \right|^2$$
(2)

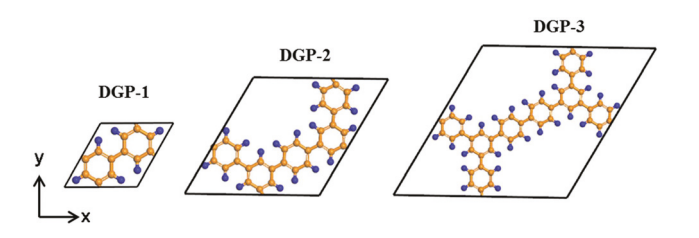


Fig. 1 The unit cells of 2D DPG: DGP-1, DGP-2, and DGP-3, where orange represents carbon atoms and blue represents hydrogen atoms. All the phenyl rings have the same size. The porosity of DPG is varied by introducing additional same-size phenyl rings in one unit

where q is the wave vector,  $\omega$  is the frequency,  $\alpha$  represents integration directions (x, y, z),  $\tau$  is the integration time, N is the total number of unit cells in the simulated supercell, B is the total number of atoms in a unit cell,  $m_h$  is the mass of atom b in the unit cell,  $\dot{u}_{\alpha}\begin{pmatrix} l \\ h \end{pmatrix}$  is the  $\alpha$ -th component of the velocity of atom b in cell l, and  $r_l$  is the equilibrium position of cell l.

#### 3. Results and discussion

#### Porosity-dependent thermal conductivity

We first obtained the thermal conductivity of DPG in zigzag and armchair directions at 300 K as shown in Fig. 2. The porosity of 2D polymers, P, is defined by

$$P = \left(\frac{\left(\frac{N}{V}\right)_{\text{graphene}} - \left(\frac{N}{V}\right)_{\text{2D polymers}}}{\left(\frac{N}{V}\right)_{\text{graphene}}}\right) \times 100\%$$
 (3)

where N and V are the total number of atoms and volume in one unit cell, respectively. We found that thermal conductivity of DPG-1 is not isotropic, while it is fairly isotropic for DPG-2 and DPG-3 due to their large porosity. Thermal conductivities of DPG-1 in zigzag and armchair direction are 84.4 ± 10.8 W m<sup>-1</sup> K<sup>-1</sup> and 110.8  $\pm$  19.6 W m<sup>-1</sup> K<sup>-1</sup>, respectively. Despite a small porosity of 3.2%, the thermal conductivities are at least one order of magnitude smaller than that of graphene with a porosity of 0%. The much lower thermal conductivity of DPG-1 can be attributed to weak single C-C bonds between phenyl rings and mass disorder originating from C and H atoms compared to tightly packed carbon atoms and pure, strong

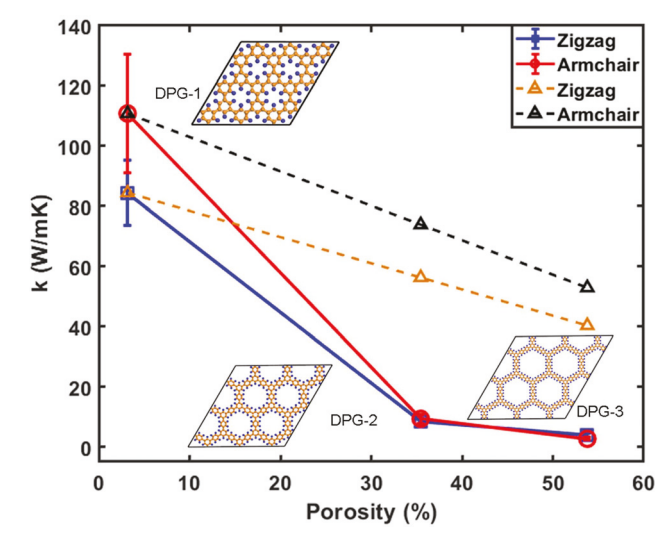


Fig. 2 Thermal conductivity (k) in zigzag (blue squares) and armchair (red circles) direction vs. porosity of DPG at 300 K. The solid black line represents results from the EMD simulation. The dashed black and orange triangles represent the calculated thermal conductivity trend due to reduced volumetric heat capacity from increasing porosity based on eqn (5).

Communication Nanoscale

 $\pi$ -conjugated bonds in graphene. Moreover, the thermal conductivity of DPG-1 is larger in the armchair direction than that in zigzag direction, which is opposite to the trend of graphene.<sup>30</sup>

To further explain the underlying mechanism, we took a closer look at the thermal conductivity equation of 2D materials:

$$k = \frac{1}{2}c_{\rm v}\bar{v}^2\bar{\tau} \tag{4}$$

where k is in-plane thermal conductivity;  $c_v$  is volumetric heat capacity;  $\bar{v}$  is the average phonon group velocity; and  $\tau$  is the phonon lifetime. Because our EMD simulation falls into the classical limit, the total volumetric heat capacity can be given by  $c_v = 3k_BN/V$ , where  $k_B$  is the Boltzmann constant, N is the number of atoms, and V is the volume. Since DPG-1 has slightly larger porosity than graphene, the  $c_v$  of DPG-1 is slightly smaller than that for graphene. To evaluate the role of phonon group velocity and phonon lifetime in thermal conductivity, we calculated the phonon dispersion of graphene and DPG-1 using the SED method as shown in Fig. 3a and b, respectively. The phonon dispersion of graphene is in good agreement with reported results.31,32 There are many more phonon branches for DPG-1 due to the greater number of atoms in the unit cell of DPG-1 compared to graphene. The most striking feature of the dispersion is the suppression of longitudinal acoustic (LA) and transverse acoustic (TA) modes. Compared to graphene, whose acoustic modes reach as high as 36 THz, the frequency of LA and TA modes of DPG-1 are below approximately 10 THz. The considerably softer acoustic modes give a much smaller phonon group velocity. Moreover, the bandwidths of the phonon dispersion curves are related to phonon lifetime. The larger the broadening of the SED peaks, the shorter the phonon lifetime.<sup>29,29</sup> Phonon dispersion of DPG-1 is more broadening than graphene, indicating a smaller phonon lifetime. Additionally, DPG-1 shows much lower optical branches and stronger overlapping between optical and acoustic modes, leading to strong acoustic-optical phonon scattering and, thus, reduced phonon lifetime. In brief, the lower phonon velocity and smaller phonon lifetime of DPG-1

are essential to generating lower thermal conductivity than graphene.

Despite the much lower thermal conductivity of DPG-1 compared to graphene, the thermal conductivity of DPG-1 is considerably high due to π-conjugation, which is higher than thermal conductivities of half of the pure metals.<sup>33</sup> However, as we increased the porosity of DPG, its thermal conductivity decreases dramatically (Fig. 2). Assuming that the only cause of the thermal conductivity reduction with increasing porosity is from the reduced density and the corresponding volumetric heat capacity, we can estimate the k of DPG-2 and DPG-3 by the following equation

$$k_{\mathrm{2D\,polymers}} = k_{\mathrm{DPG-1}} \times \left(\frac{N}{V}\right)_{\mathrm{2D\,polymers}} / \left(\frac{N}{V}\right)_{\mathrm{DPG-1}}$$
 (5)

We expect a decreasing trend as shown by the dashed line in Fig. 2. However, DPG-2 and DPG-3 have averaged  $k((k_x + k_y)/2)$  of  $8.8 \pm 0.7 \text{ W m}^{-1} \text{ K}^{-1}$  and  $3.3 \pm 0.4 \text{ W m}^{-1} \text{ K}^{-1}$ , respectively, which are much smaller than estimated values. Therefore, there must be other effects dominating the thermal conductivity reduction.

Further examination of the structures of DPG-1, DPG-2, and DPG-3 unveils that there are two other major effects besides density reduction: chain alignment and segmental rotation. The structures of DPG are shown in Fig. 4. Phenyl rings of DPG-1 form a weak zigzag along the x direction for heat conduction, while DPG-3 has a strong zigzag along the x direction due to increasing spatial extension between the vertices resulting from high porosity (Fig. 4a). Similarly, the heat conduction path along the y direction in DPG-1 is straighter compared to that along the y direction in DPG-3. Intuitively, there should be more impedance in phonon conduction when the conduction paths are not straight and keep changing directions. Therefore, the straighter path in DPG-1 is more favorable to heat conduction. In addition, DPG-1 is totally flat due to its densely packed structure, while the central phenyl rings between two vertex rings in DPG-3 can rotate out of the plane to form an energetically favorable geometry (Fig. 4b). We intro-

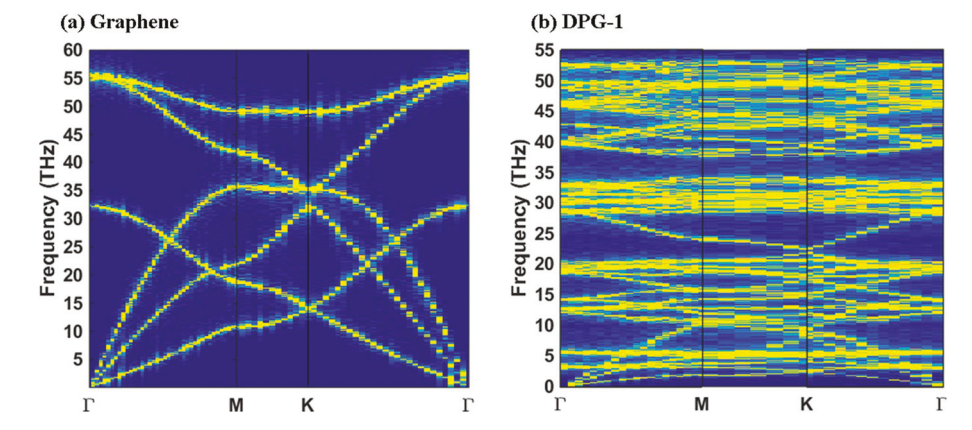


Fig. 3 Phonon dispersion calculated by the SED method. (a) graphene; (b) DPG-1.

Nanoscale Communication

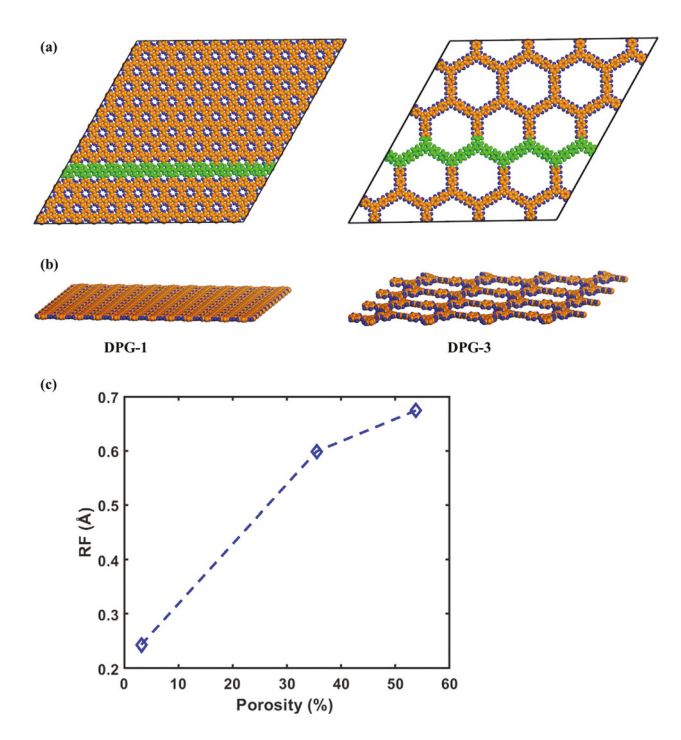


Fig. 4 Schematics of DPG-1 and DPG-3 structures; (a) top view, green denotes a single chain along the x direction. DPG-1 shows high alignment, while DPG-3 shows a zigzag shape. (b) Side view. DPG-1 shows a totally flat structure, while DPG-3 has segmental rotations. (c) Rotation factor of DPG as a function of porosity at 300 K.

duced a new rotation factor (RF) to quantify the rotation level of a DPG in an *x*–*y* plane:

$$RF = \frac{1}{N} \sum_{i}^{N} \sigma(Z) \tag{6}$$

where Z denotes z coordinates of all the atoms in a Cartesian coordinate system, and  $\sigma(Z)$  denotes its standard deviation, i denotes the  $i^{\text{th}}$  snapshot from atomic position dump file during an NVE ensemble, N is the total number of snapshots from the dump file and N=40 in this study. Note that this is the first time RF has been used and the RF is applicable for all 2D structures in an x-y plane. The RF increases with the porosity increases as shown in Fig. 4c. This rotational disorder not only can introduce more scattering and reduce phonon lifetimes but also can reduce bond strength because of the reduced overlapping of the p-orbital of  $\pi$ -conjugated bonds among the phenyl rings.

To further support these structural effects, we obtained the phonon dispersion of DPG along the  $\Gamma$  to M direction as shown in Fig. 5. Phonon dispersion curves are significantly broadened from DPG-1 to DPG-3, indicating decreasing phonon lifetimes. In addition, the LA and TA branches are further softened with increasing porosity, which represents reduced group velocity. The estimation of average phonon group velocities and average phonon mean free paths as well as the plots of phonon group velocity and phonon mean free path as a function of porosity and RF can be found in the

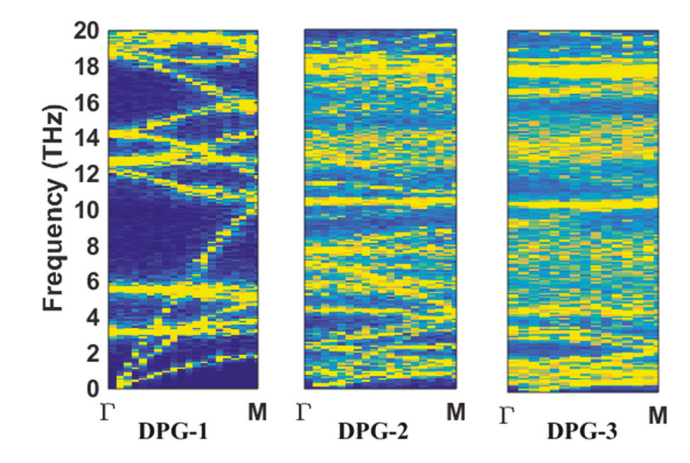


Fig. 5 Phonon dispersion of DPG-1, DPG-2, and DPG-3 in the  $\Gamma$  to M direction calculated by the SED method.

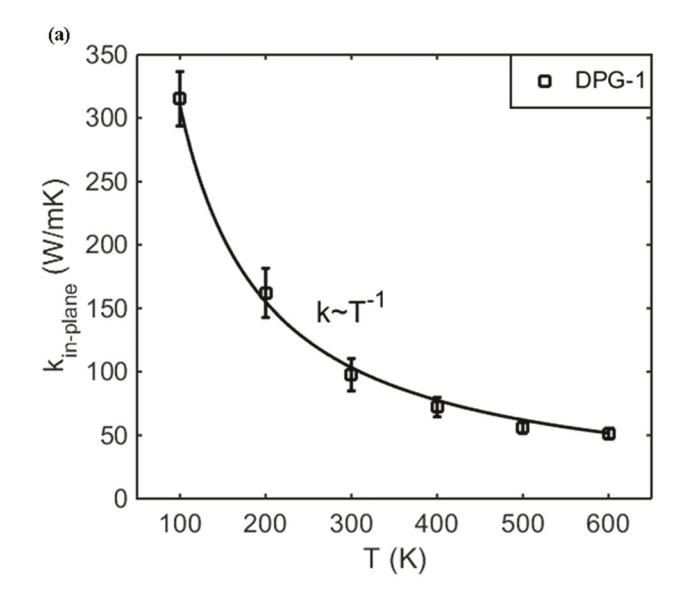
ESI.† In brief, reduced volumetric heat capacity originating from reduced density, decreased phonon lifetime, and lower phonon velocity is essential to the unexpectedly fast decreasing trend of thermal conductivity for DPG.

DPG can be viewed as 2D covalently bonded PPP. Singlechain PPP was reported to have a thermal conductivity of  $\sim 50$ W m<sup>-1</sup> K<sup>-1</sup> at 300 K,<sup>34</sup> and crystalline PPP (single-chain periodically repeating in 3D) gave a thermal conductivity of ~45 W m<sup>-1</sup> K<sup>-1</sup> at 300 K.<sup>35</sup> The relatively large thermal conductivity was attributed to the rigid backbone of PPP suppressing segmental rotation and, thus, phonon scattering due to overlap of the p-orbitals in  $\pi$ -conjugated polymers.<sup>35</sup> Interestingly, DPG-1 shows 2 times higher thermal conductivity than single-chain or crystalline PPP. The densely packed structure and low porosity of DPG-1 lead to highly aligned chains and less segmental rotation, which increase overlap of the p-orbitals to form strong  $\pi$ -conjugated bonds. Moreover, DPG-1 has 2D covalent bonds, while single-chain and crystalline PPP have covalent bonding along one direction only. On the other hand, DPG-2 and DPG-3 give much lower thermal conductivity than singlechain or crystalline PPP due to increased chain alignment disorder and higher segmental rotation. Our results demonstrate, for the first time, that  $\pi$ -conjugated polymers can give high or low thermal conductivity depending on their structural orientation.

#### 3.2 Temperature-dependent thermal conductivity

We calculated the temperature dependent thermal conductivity of DPG as shown in Fig. 6. The in-plane thermal conductivity is averaged between the zigzag and armchair directions. Between 100 and 600 K, DPG-1 shows a clear  $T^{-1}$  dependence of thermal conductivity, which is a typical characteristic of crystalline materials. This  $T^{-1}$  dependence results from the more frequent anharmonic Umklapp process and, hence, decreased phonon lifetimes as temperature increases. Interestingly, DPG-2 and DPG-3 show much weaker temperature dependence of  $(AT + B + C/T)^{-1}$ , which indicates a combination of crystalline and glassy phases.  $^{36,37}$  The change of

Communication Nanoscale



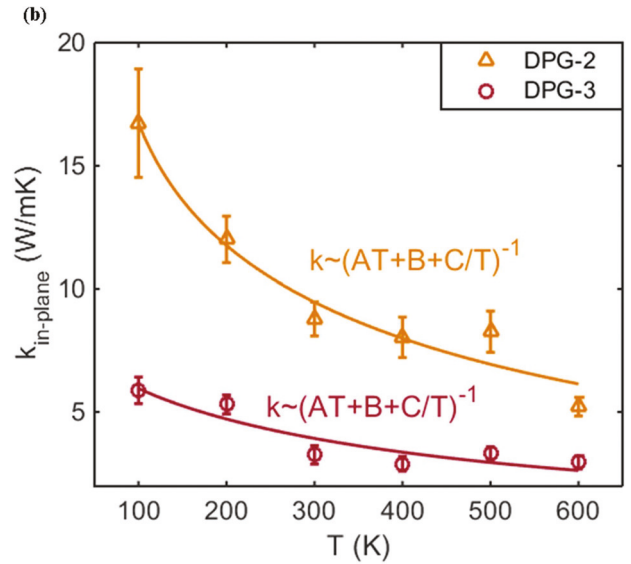


**Fig. 6**  $k_{\text{in-plane}}$  as a function of temperature T (K); (a) DPG-1, black line denotes  $\sim T^{-1}$  fitting. (b) DPG-2 and DPG-3, orange and red lines represent  $(AT + B + C/T)^{-1}$  fitting; A, B and C are constants.

temperature-dependent thermal conductivity reveals a decrease of crystallinity in DPG with an increase in porosity, which reiterates the decreased chain alignment and the increased segmental rotations.

## 4. Conclusion

We studied in-plane thermal conductivity of  $\pi$ -conjugated DPG using the EMD method. We found that DPG gives at least one order of magnitude lower thermal conductivity than graphene. The thermal conductivity of DPG decreases with increasing porosity, which is attributed to not only reduced heat capacity resulting from lower density but also to decreased phonon lifetime and group velocity originating from increased chain dis-

order and segmental rotation. Moreover, we demonstrated that the thermal conductivity of low-porosity DPG is two times higher than that of single-chain or crystalline  $\pi$ -conjugated PPP, while high-porosity DPG gives unexpectedly low thermal conductivity. This highlights, for the first time, that even  $\pi$ -conjugated 2D polymers can have very low thermal conductivity. DPG-1 shows  $T^{-1}$  temperature-dependent thermal conductivity at 100–600 K, indicating high crystallinity. DPG-2 and DPG-3 show much weaker temperature dependence than DPG-1, revealing the decrease in crystallinity of DPG. The knowledge gained from this study can be applied to tune the thermal conductivity of 2D polymers for various applications.

#### Conflicts of interest

There are no conflicts to declare.

## Acknowledgements

This work was funded by NSF CEBT-1641103. This work used the Extreme Science and Engineering Discovery Environment (XSEDE), which is supported by National Science Foundation grant number ACI-1053575. This research used resources of the Oak Ridge Leadership Computing Facility, which is a DOE Office of Science User Facility supported under Contract DE-AC05-00OR22725. The authors also acknowledge Advanced Research Computing at Virginia Tech for providing computational resources and technical support.

### References

- N. Zhang, T. Wang, X. Wu, C. Jiang, T. Zhang, B. Jin, H. Ji,
   W. Bai and R. Bai, ACS Nano, 2017, 11, 7223-7229.
- 2 W. Liu and K. P. Loh, Acc. Chem. Res., 2017, 50, 522-526.
- 3 F. R. Dmitrii and F. Perepichka, *Science*, 2009, **323**, 216–217.
- 4 C.-Z. G. Xuan-He Liu, D. Wang and L.-J. Wan, *Adv. Mater.*, 2014, **26**, 6912–6920.
- 5 M. P. Renhao Dong, H. Liang, Z. Zheng, X. Zhu, J. Zhang and X. Feng, *Angew. Chem., Int. Ed.*, 2015, 54, 12058–12063.
- 6 Z. Zheng, R. Grünker and X. Feng, Adv. Mater., 2016, 28, 6529–6545.
- 7 Y. Hong, J. Zhang and X. C. Zeng, *Nanoscale*, 2018, 10, 4301–4310.
- 8 M. Bieri, M. Treier, J. Cai, K. Aït-Mansour, P. Ruffieux, O. Gröning, P. Gröning, M. Kastler, R. Rieger and X. Feng, *Chem. Commun.*, 2009, 6919–6921.
- 9 M. Bieri, M.-T. Nguyen, O. Gröning, J. Cai, M. Treier, K. Aït-Mansour, P. Ruffieux, C. A. Pignedoli, D. Passerone, M. Kastler, K. Müllen and R. Fasel, *J. Am. Chem. Soc.*, 2010, 132, 16669–16676.
- 10 R. Gutzler and D. F. Perepichka, *J. Am. Chem. Soc.*, 2013, 135, 16585–16594.

Nanoscale

- 11 A. Du, Z. Zhu and S. C. Smith, *J. Am. Chem. Soc.*, 2010, **132**, 2876–2877.
- 12 Y. Ding, Y. Wang, S. Shi and W. Tang, *J. Phys. Chem. C*, 2011, 115, 5334–5343.
- 13 R. Lu, Z. Meng, E. Kan, F. Li, D. Rao, Z. Lu, J. Qian, C. Xiao, H. Wu and K. Deng, *Phys. Chem. Chem. Phys.*, 2013, 15, 666–670.
- 14 Y. Li, Z. Zhou, P. Shen and Z. Chen, *Chem. Commun.*, 2010, **46**, 3672–3674.
- 15 See http://accelrys.com/products/materials-studio/for Accelrys Software and M. S. v. Inc.
- 16 R. Gutzler, Phys. Chem. Chem. Phys., 2016, 18, 29092-29100.
- 17 J.-R. Hill and J. Sauer, J. Phys. Chem., 1995, 99, 9536-9550.
- 18 K.-S. Chang, T. Yoshioka, M. Kanezashi, T. Tsuru and K.-L. Tung, *Chem. Commun.*, 2010, **46**, 9140–9142.
- 19 H. Ma and Z. Tian, Appl. Phys. Lett., 2017, 110, 091903.
- 20 C. Li, H. Ma and Z. Tian, Appl. Therm. Eng., 2017, 111, 1441–1447.
- 21 H. Ma and Z. Tian, Nano Lett., 2018, 18, 43-48.
- 22 H. Ma and Z. Tian, Appl. Phys. Lett., 2015, 107, 073111.
- 23 S. Plimpton, J. Comput. Phys., 1995, 117, 1-19.
- 24 M. S. Green, J. Chem. Phys., 1952, 20, 1281-1295.

- 25 M. S. Green, J. Chem. Phys., 1954, 22, 398-413.
- 26 H. Babaei and C. E. Wilmer, Phys. Rev. Lett., 2016, 116, 025902.
- 27 A. B. Robbins and A. J. Minnich, Appl. Phys. Lett., 2015, 107, 201908.
- 28 B. Qiu and X. Ruan, Appl. Phys. Lett., 2012, 100, 193101.
- 29 X. Qian, X. Gu and R. Yang, Appl. Phys. Lett., 2016, 108, 063902.
- 30 Y. Hong, J. Zhang, X. Huang and X. C. Zeng, *Nanoscale*, 2015, 7, 18716–18724.
- 31 L. Falkovsky, J. Exp. Theor. Phys., 2007, 105, 397-403.
- 32 Z. Wang and X. Ruan, J. Appl. Phys., 2017, 121, 044301.
- 33 S. Shen, A. Henry, J. Tong, R. Zheng and G. Chen, *Nat. Nano*, 2010, 5, 251–255.
- 34 J. Liu and R. Yang, *Phys. Rev. B: Condens. Matter Mater. Phys.*, 2012, **86**, 104307.
- 35 T. Zhang, X. Wu and T. Luo, J. Phys. Chem. C, 2014, 118, 21148-21159.
- 36 W. N. dos Santos, J. A. de Sousa and R. Gregorio Jr., *Polym. Test.*, 2013, 32, 987–994.
- 37 W. D. Kingery and M. C. McQuarrie, *J. Am. Ceram. Soc.*, 1954, 37, 67–72.